

Article

Reliability of inference of directed climate networks using conditional mutual information

Jaroslav Hlinka ^{1,*}, David Hartman ¹, Martin Vejmelka ¹, Jakob Runge ^{2,3}, Norbert Marwan ², Jürgen Kurths ^{2,3,4} and Milan Paluš ¹

¹ Institute of Computer Science, Academy of Sciences of the Czech Republic, Pod vodarenskou vezi 2, 182 07, Prague 8, Czech Republic

² Potsdam Institute for Climate Impact Research (PIK), 14473 Potsdam, Germany

³ Department of Physics, Humboldt University, 12489 Berlin, Germany

⁴ Institute for Complex Systems and Mathematical Biology, University of Aberdeen, Aberdeen AB24 3UE, United Kingdom

* Author to whom correspondence should be addressed; hlinka@cs.cas.cz, (+420) 266053808

Version January 29, 2013 submitted to *Entropy*. Typeset by *LaTeX* using class file *mdpi.cls*

1 **Abstract:** Across geosciences, many investigated phenomena relate to specific complex
2 systems consisting of intricately intertwined interacting subsystems. Such dynamical com-
3 plex systems can be represented by a directed graph, where each link denotes an existence
4 of a causal relation, or information exchange between the nodes. For geophysical systems
5 such as global climate, these relations are commonly not known theoretically but estimated
6 from recorded data using causality analysis methods. These include bivariate nonlinear
7 methods based on information theory and their linear counterpart. A trade-off between
8 the valuable sensitivity of nonlinear methods to more general interactions and potentially
9 higher numerical reliability of linear method may affect inference regarding structure
10 and variability of climate networks. We investigate the reliability of directed climate
11 networks detected by selected methods and parameter settings, using stationarized model
12 of dimensionality-reduced surface air temperature data from reanalysis of 60-year global
13 climate records. Overall, all studied bivariate causality methods provided reproducible
14 estimates of climate causality networks; with linear approximation showing higher reliability
15 than the investigated nonlinear methods. On the example dataset, optimizing the investigated
16 nonlinear methods with respect to reliability increased similarity of the detected networks
17 to their linear counterparts, supporting the particular hypothesis of surface air temperature
18 climate reanalysis data near-linearity.

Keywords: causality; climate; nonlinearity, transfer entropy, network, stability

1. Introduction

Across geosciences, many investigated phenomena relate to specific complex systems consisting of intricately intertwined interacting subsystems. These can be suitably represented as networks, an approach that is gaining increasing attention in complex systems community [1,2]. The meaning of the existence of a link between nodes of a network depends on the area of application, but in many cases it is related to some form of information exchange between the nodes.

This approach has already been adopted for the analysis of various phenomena in the global climate system [3–7]. Typically, a graph is constructed by considering two locations linked by a connection, if there is an instantaneous dependence between the localized values of a variable of interest.

This dependence can be conveniently quantified by mutual information - an entropy-based general measure of statistical dependence that takes into account nonlinear contributions to the coupling. In practice, for reasons of theoretical and numerical simplicity, linear Pearson's correlation coefficient might be sufficient, although potentially neglecting the nonlinear contributions to interactions. In particular, while initial works by Donges et al. stressed the role of mutual information in detecting important features of global climate networks [8,9], more detailed recent work has shown that the differences between correlation and mutual information graphs are mostly (but not necessarily completely) spurious, such as due to natural and instrumental (related to data collection) nonstationarities of the data [10].

However, these methods do not allow to assess the directionality of the links and of the underlying information flow. This motivates the use of more sophisticated measures, known also as causality analysis methods.

The family of causality methods include linear approaches such as the Granger causality analysis [11] as well as more general nonlinear methods. A prominent representative of nonlinear causality assessment method is the conditional mutual information [12] known also as transfer entropy [13].

Arguably, the nonlinear methods, due to their model-free nature, have the theoretical advantage of being sensitive to forms of interactions that linear methods may detect only partially or not at all. On the other side, this advantage might be more than outweighed by a potentially lower precision. Depending on specific circumstances, this may adversely affect the reliability of detection of network patterns.

Apart from uncertainty about the general network pattern, reliability is important when the interest is in detecting changes in time, with the need to distinguish them from random variance of the estimates among different sections of time series under investigation - a task that is relevant in many areas of geoscience including climate research.

In other words, before analyzing a complex dynamical system using network theory, a key initial question is that of the reliability of the network construction, and of its dependence on the causality method choice and settings.

55 We study this question for a selection of standard causality methods, using a timely application in
 56 the study of climate network and its variability. In particular, surface air temperature data from the
 57 NCEP/NCAR reanalysis dataset [14,15] are used. The original data contain more than 10,000 time
 58 series - a relatively dense grid covering the whole globe. For efficient computation and visualization of
 59 the results, it is convenient to reduce the dimensionality of the data. We use principal component analysis
 60 and select only components that have significantly high explained variance compared to corresponding
 61 spatially independent but temporally dependent (i.e. ‘colored’) random noise.

62 As the causality network construction reliability may crucially depend on the specific choice of the
 63 causality estimator, we quantitatively assess the effect of choice of different causality measures and their
 64 parametrization.

65 We assess the network construction reliability by quantifying the similarity of causality matrices
 66 reconstructed from independent realization of a stationary model of data. These realizations are either
 67 independently generated, or they represent individual non-overlapping temporal windows in a single
 68 stationary realization. Optimal parameter choice of the applied nonlinear methods is detected, and the
 69 reliability of networks constructed using linear and nonlinear methods compared.

70 The latter method, i.e. comparing networks reconstructed from temporal windows, allows to assess
 71 the network variability on real data and compare it with variability on the stationary model.

72 2. Data and Methods

73 2.1. Causality assessment methods

74 2.1.1. Granger causality analysis

75 A prominent method for assessing causality is so-called Granger causality analysis, named after Sir
 76 Clive Granger, who proposed this approach to time series analysis in a classical paper [11]. However, the
 77 basic idea can be traced back to Wiener [16], who proposed that if the prediction of one time series can
 78 be improved by incorporating the knowledge of a second time series, then the latter can be said to have a
 79 causal influence on the former. This idea was formalized by Granger in the context of linear regression
 80 models. In the following, we outline the methods of assessment of Granger causality, following the
 81 description given in [17] and [18,19].

82 Consider two stochastic processes X_t and Y_t and assume they are jointly stationary. Let further the
 83 autoregressive representations of each process be:

$$X_t = \sum_{j=1}^{\infty} a_{1j} X_{t-j} + \epsilon_{1t}, \quad \text{var}(\epsilon_{1t}) = \Sigma_1, \quad (1)$$

$$Y_t = \sum_{j=1}^{\infty} d_{1j} Y_{t-j} + \eta_{1t}, \quad \text{var}(\eta_{1t}) = \Gamma_1, \quad (2)$$

84 and the joint autoregressive representation be:

$$X_t = \sum_{j=1}^{\infty} a_{2j} X_{t-j} + \sum_{j=1}^{\infty} b_{2j} Y_{t-j} + \epsilon_{2t}, \quad (3)$$

$$Y_t = \sum_{j=1}^{\infty} c_{2j} X_{t-j} + \sum_{j=1}^{\infty} d_{2j} Y_{t-j} + \eta_{2t}, \quad (4)$$

85 where the covariance matrix of the noise terms is:

$$\Sigma = \text{Cov} \begin{pmatrix} \epsilon_{2t} \\ \eta_{2t} \end{pmatrix} = \begin{pmatrix} \Sigma_2 & \Lambda_2 \\ \Lambda_2 & \Gamma_2 \end{pmatrix}. \quad (5)$$

The causal influence from Y to X is then quantified based on the decrease in the residual model variance when we include the past of Y in the model of X , i.e. when we move from the independent model given by Equation (1) to the joint model given by Equation (3):

$$F_{Y \rightarrow X} = \ln \frac{\Sigma_1}{\Sigma_2}. \quad (6)$$

Similarly, the causal influence from X to Y is defined as:

$$F_{X \rightarrow Y} = \ln \frac{\Gamma_1}{\Gamma_2}. \quad (7)$$

86 Clearly, the causal influence defined in this way is always nonnegative.

87 The original introduction of the concept of statistical inference of causality [11] includes a third
88 (potentially highly multivariate) process Z , representing all the other intervening process that should be
89 controlled for in assessing the causality between X and Y . The bivariate (or ‘pairwise’) implementation
90 of the estimator thus constitutes a computational simplification of the original process, for the sake
91 of numerical stability as well as comparability to the bivariate transfer entropy (conditional mutual
92 information) approach introduced later. See section 4 for further discussion of related issues.

93 2.2. Estimation of GC

94 Practical estimation of the Granger causality involves fitting the full and depleted models described
95 above to experimental data. While the theoretical framework outlined above is formulated in terms of
96 infinite sums, the fitting procedure requires selection of the model order p for the models. For our report,
97 we have selected $p = 1$ to allow direct comparability of the Granger causality analysis to the nonlinear
98 methods considered later. This choice is the most common choice for Granger causality in literature and
99 amounts to looking for links with lag 1 time unit.

100 2.3. Transfer entropy

101 To provide a framework for discussion of the related issues, it is useful to consider that for a general
102 bivariate stochastic process the Granger causality concept, can be captured in information-theoretic
103 terms. In particular, we can define that X causes Y if the knowledge of past of X decreases

104 the uncertainty about Y (above what the knowledge of past of Y and potentially all other relevant
 105 confounding variables already informs). This simple concept is captured in the definition of *transfer*
 106 *entropy* (TE, [13]). TE as can be defined in terms of *conditional mutual information* as shown below,
 107 following closely [12].

For two discrete random variables X, Y with sets of values Ξ and Υ and probability distribution functions (PDFs) $p(x), p(y)$ and joint PDF $p(x, y)$, the Shannon entropy $H(X)$ is defined as

$$H(X) = - \sum_{x \in \Xi} p(x) \log p(x), \quad (8)$$

and the joint entropy $H(X, Y)$ of X and Y as

$$H(X, Y) = - \sum_{x \in \Xi} \sum_{y \in \Upsilon} p(x, y) \log p(x, y). \quad (9)$$

The conditional entropy $H(X|Y)$ of X given Y is

$$H(X|Y) = - \sum_{x \in \Xi} \sum_{y \in \Upsilon} p(x, y) \log p(x|y). \quad (10)$$

The amount of common information contained in the variables X and Y is quantified by the mutual information $I(X; Y)$ defined as

$$I(X; Y) = H(X) + H(Y) - H(X, Y). \quad (11)$$

The conditional mutual information $I(X; Y|Z)$ of the variables X, Y given the variable Z is given as

$$I(X; Y|Z) = H(X|Z) + H(Y|Z) - H(X, Y|Z). \quad (12)$$

108 Entropy and mutual information are measured in bits if the base of the logarithms in their definitions
 109 is 2. It is straightforward to extend these definitions to more variables, and to continuous rather than
 110 discrete variables.

111 Transfer entropy from process X_t to process Y_t then corresponds to the conditional mutual information
 112 between X_t and Y_{t+1} conditional on Y_t :

$$T_{X \rightarrow Y} = I(X_t, Y_{t+1} | Y_t). \quad (13)$$

113 While the definition of these information-theoretic functionals describing dependence structure
 114 between variables is very general and elegant, the practical estimation faces challenges related to the
 115 problem of efficient estimation of the PDF of the studied variables from samples of finite size. For the
 116 further considerations, it is important to bear in mind the distinction between the true quantities of the
 117 underlying stochastic process, and their finite-sample estimators.

118 2.4. Potential causes of observed difference

Interestingly, it can be shown that for linear Gaussian processes, transfer entropy is equivalent to linear Granger causality, up to a multiplicative factor [20]:

$$\mathcal{T}_{X \rightarrow Y} = \frac{1}{2} \mathcal{F}_{X \rightarrow Y}. \quad (14)$$

119 However, in practice, the estimates of transfer entropy and linear Granger causality may differ.
 120 There are principally two main reasons for this divergence between the results. Firstly, when the
 121 underlying process is not linear Gaussian, the true transfer entropy may differ from the true linear
 122 Granger causality corresponding to the linear approximation of the process. A second reason for
 123 divergence between sample estimates of transfer entropy and linear Granger causality, valid even for
 124 linear Gaussian processes, is the difference in the properties of the estimators of these two quantities, in
 125 particular bias and variance of the estimates.

126 2.5. TE estimation

127 There are many algorithms for estimation of information-theoretical functionals, that can be adapted
 128 to compute transfer entropy estimates. Two basic classes of nonparametric methods for the estimation of
 129 conditional mutual information are the *binning methods* and the *metric methods*. The former discretize
 130 the space in to regions usually called bins or boxes - a robust example is the equiquantal method, based
 131 on discretization of studied variables into Q equiquantal bins (EQQ, [21]). In the latter methods, the
 132 probability distribution function estimation depends on distances between the samples computed using
 133 some metric. An example of a metric method is the k -nearest neighbor (kNN, [12]) algorithm. For more
 134 detail on methods of estimation of conditional mutual information and their comparison see [12].

135 Note that both these algorithms require setting an additional parameter. While some heuristic
 136 suggestions have been published in the literature, the suitable values of the parameters may depend
 137 on specific aspects of the application including the character of the time series. For the purpose of this
 138 study, we use a range of parameter values and subsequently select the parameter values providing the
 139 most stable results for further comparison with linear methods, see below.

140 2.6. Data

141 2.6.1. Dataset

142 Data from the NCEP/NCAR reanalysis dataset [14] have been used. In particular, we utilize the time
 143 series $x_i(t)$ of the daily and monthly mean surface air temperature from January 1948 to December 2007
 144 ($T_d = 21900$ and $T_m = 720$ time points respectively), sampled at latitudes λ_i and longitude ϕ_i forming a
 145 regular grid with a step of $\Delta\lambda = \Delta\phi = 2.5^\circ$. The points located at the globe poles have been removed,
 146 giving a total of $N = 10224$ spatial sampling points.

147 2.6.2. Preprocessing

148 To minimize the bias introduced by periodic changes in the solar input, the mean annual cycle is
149 removed from the data to produce so-called anomaly time series. The data were further standardized so
150 that the time series at each grid point has unit variance. The time series are then scaled by the cosine
151 of the latitude to account for grid points closer to the poles representing smaller areas and being closer
152 together (thus biasing the correlation with respect to grid points farther apart). The poles are thus omitted
153 entirely by effectively removing data for latitude ± 90 .

154 2.6.3. Computing the components

155 The covariance matrix of the scaled time series obtained by preprocessing is computed. Note that this
156 covariance matrix is equal to the correlation matrix, where each correlation is scaled by the inverse of
157 the product of the cosines of the latitudes of the time series entering the correlation.

158 Next, the eigendecomposition of the covariance matrix is computed. The eigenvectors corresponding
159 to genuine components are extracted (estimation of the number of components is explained in the next
160 paragraph). The eigenvectors are then rotated using the VARIMAX method [22].

161 The rotated eigenvectors are the resulting components. Each component is represented by a scalar
162 field of intensities over the globe, and by a corresponding representative time series. See Figure 6 for a
163 parcellation of the globe by the components. For each location, the color corresponding to the component
164 with maximal intensity is used - due to good spatial localization and smoothness of the components this
165 leads to parcellation of the globe into generally contiguous regions.

166 2.6.4. Estimating the dimensionality of the data

167 To reduce the dimensionality, only a subset of the components is selected for further analysis. The
168 main idea rests in determining significant components by comparing the eigenvalues computed from the
169 original data to eigenvalues computed from a control dataset corresponding to the null hypothesis of
170 uncoupled time series with the same temporal structure as the original data. To accomplish this, the time
171 series in the control datasets are generated as realizations of autoregressive (AR) models fit to each time
172 series independently. The dimension of the AR process is estimated for each time series separately using
173 the Bayesian Information Criterion [23].

174 This model is used to generate 10000 realizations in the control dataset. The eigendecomposition of
175 each realization is computed and aggregated so a distribution of each eigenvalue (1st, 2nd, ...) is available
176 under the null hypothesis.

177 Finding the significant eigenvalues then reduces to a multiple comparison problem which we resolved
178 using the False Discovery Rate (FDR) technique [24] which has led to the identification of 67 genuine
179 components.

180 For computational reasons, the decomposition was carried out on the monthly data and the component
181 spatial distributions were used to extract daily time series from correspondingly preprocessed daily data
182 (anomalization, standardization, cosine transform). The method thus yielded full-resolution component
183 localization on the 10224-point grid while also providing a high-resolution time series associated with
184 each component.

185 2.7. Network construction

186 Formally, in the graph-theoretical approach a network is represented by an graph $G = (V, E)$, where
187 V is the set of nodes of G , $n = \#V$ is the number of nodes and $E \subset V^2$ is the set of the edges (or links)
188 of G . In weighted graphs, each edge connecting nodes i and j can be assigned a weight $a_{i,j}$ representing
189 the strength of the link. Thus, the causality matrix \mathcal{T} having as its entries the pairwise causalities $\mathcal{T}_{i,j} =$
190 $\mathcal{T}_{X_i \rightarrow X_j}$ can be understood as a weighted graph with variable strength of links. Commonly, the graph is
191 transformed into an unweighted matrix by suitable thresholding, keeping only links with weights higher
192 than some threshold (and setting their weights to 1), while removing all the weaker links (setting the
193 weights to zero).

194 There are three principal strategies to choose the threshold - either a fixed value based on expert
195 judgment of what constitutes a strong link, or adaptively to enforce a required density of the graph
196 (relative number of links with respect to the maximum number possible, i.e. in a full graph of given
197 size). The third option is to use statistical testing to detect statistically significant links.

198 In the current paper, we start with the original unthresholded graphs, but provide also example results
199 for thresholded graphs using the above named approaches.

200 2.8. Reliability assessment

201 In line with the terminology of psychometrics or classical test theory, by reliability we mean the
202 overall consistency of a measure (consistency here not meant in the statistical sense of asymptotic
203 behavior). In the context of network construction, we considered a method reliable if the networks
204 constructed by its means from different samples of the same dynamical process would be similar to
205 each other. Note that this does not necessarily imply validity or accuracy of the method - under some
206 circumstances, a method could consistently arrive at wrong results. In a way, reliability/consistency can
207 be considered a first step to validity. In practical terms, even if the validity was undoubted, reliability
208 can give the researcher an estimate on the confidence he/she can have in reproducibility of the results.

209 To assess similarity of two matrices, many methods are available, including (entry-wise) Pearson's
210 linear correlation coefficient. Inspection of the causality matrices suggests heavily non-normal
211 distribution of the values with many outliers. Therefore, the correlation of ranks, using Spearman's
212 correlation coefficient, may be more suitable.

213 Apart from reliability of the full weighted causality graphs, we also study the unweighted graphs
214 derived by thresholding. Based on inspection of the causality matrices, a density of 0.01 (keeping 1
215 percent of strongest links) was chosen for the analysis.

216 To assess the similarity of two binary matrices, we use the Jaccard similarity coefficient. This is the
217 relative number of links that are shared by the matrices with respect to the total number of links that
218 appear at least in one of the matrices. Such a ratio is a natural measure of matrix overlap, ranging from
219 0 for matrices with no common links to 1 for identical matrices.

220 2.8.1. Model

221 A convenient method of assessing the reliability of a method on time series is to compare the results
222 obtained on different sections (temporal windows) of that time series. However, dissimilarity among the
223 results can be theoretically attributed both to lack of reliability of the method as well as to hypothetical
224 true changes in the underlying systems over time (nonstationarity).

225 Therefore, to isolate the effect of method properties, we test the methods on a realistic, but stationary
226 model of the data.

227 To provide such a stationary model of the potentially non-stationary data, a so-called surrogate data
228 was constructed.

229 Technically, the surrogate data are conveniently constructed as multivariate Fourier transform (FT)
230 surrogates [25,26]; i.e. obtained by computing the Fourier transform of the series, keeping unchanged
231 the magnitudes of the Fourier coefficients (the amplitude spectrum), but adding the same random number
232 to the phases of coefficients of the same frequency bin; the inverse FT into the time domain is then
233 performed.

234 The surrogate data represent a realization of a linear stationary process conserving the linear structure
235 (covariance and autocovariance) of the original data, and hence also the linear component of causality.
236 Note that any nonlinear component of causality should be removed, and the nonlinear methods should
237 therefore converge to the linear ones (as discussed in section 2.1).

238 After testing the reliability on the stationary linear model, we assess the stability of the methods also
239 on the real data. The variability here should reflect a mixture of method in-reliability and true climate
240 changes. Note that also the nonlinear methods may potentially diverge from the linear, as there may be
241 strictly nonlinear component of the causalities in real data.

242 2.8.2. Implementation details

243 For estimation, both the stationary model and real data time series were split into 6 windows (one for
244 each decade, i.e. with approximately 3650 time points). For each of the windows, causality matrix has
245 been computed with several causality methods.

246 In particular, we have used pairwise Granger causality as a representative linear method, and
247 conditional mutual information (transfer entropy) computed by two standard algorithms, using a range
248 of critical parameter values. The first is an algorithm based on discretization of studied variables into Q
249 equiquantal bins (EQQ, [21], $Q \in \{2, 3, 4, 5, 6, 7, 8, 9, 10, 11, 12, 13, 14\}$) and the second is a k -nearest
250 neighbor algorithm (kNN, [12], $k \in \{2, 4, 8, 16, 32, 64, 128, 256, 512\}$).

251 Each of these algorithms provides a matrix of causality estimates among the 67 climate components
252 within the respective decade. We further assess the similarity of these matrices both across time and
253 methods; first in stationary data (where temporal variability is attributable to method instability only) and
254 subsequently in real data. Apart from direct visualization, the similarity of constructed causality matrices
255 is quantified by the Spearman's rank correlation coefficient of off-diagonal entries. The reliability is
256 then estimated as the average Spearman's rank correlation coefficient across all $(6 * 5)/2 = 15$ pairs of
257 temporal windows.

258 To inspect the robustness of the results, the analysis was repeated with several possible alterations
259 to the paradigm. Firstly, the similarity among the thresholded rather than unweighted graphs was
260 assessed by the means of the Jaccard similarity coefficient instead of Spearman's rank correlation
261 coefficient. Secondly, we repeated the analysis using linear multivariate AR(1) process for generation
262 of the stationary model, instead of Fourier surrogates. Thirdly, the analysis was repeated on subsampled
263 data (by averaging each 6 days to give one data point). This way, the same methods should provide
264 causality on a longer time scale. To keep the same (and sufficiently high) number of time points, the
265 subsampled data were not split into windows, but 6 realizations were generated from a fitted multivariate
266 AR(1) process.

267 Finally, to assess the role the different reliability of the methods might have for statistical inference,
268 for selected methods we have tested the number of links that it was able to statistically distinguish
269 compared to an empirical distribution corresponding to independent linear processes. This null
270 hypothesis was realized by computing the causalities on a set of $N=19$ univariate Fourier surrogates.
271 Under the hypothesis of no dependence between the processes, the probability of the data causality value
272 for a given pair of variables being the highest from the total 20 values available is $p = 0.05$, providing a
273 convenient nonparametric test of causality.

274 3. Results

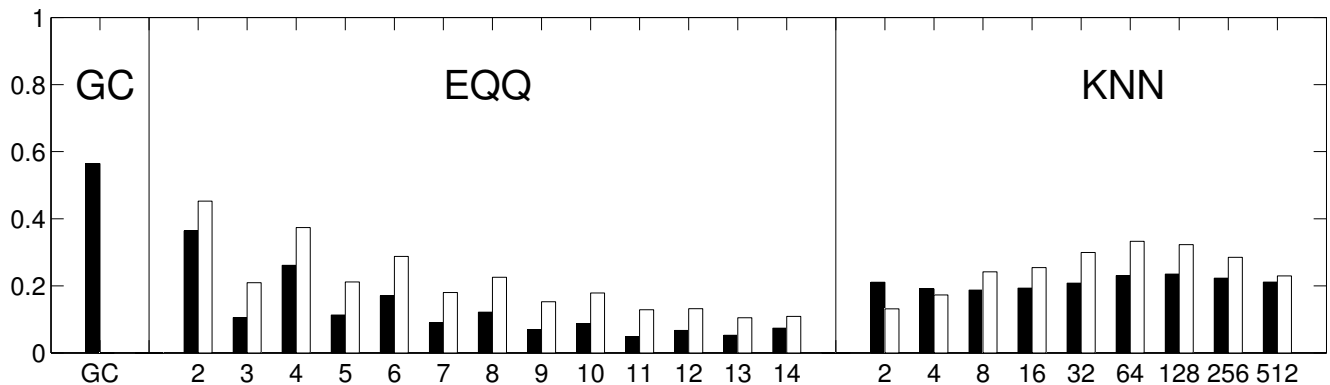
275 3.1. Weighted causality networks

276 The reliability of weighted causality networks computed from a decade of stationary model data is
277 shown in Figure 1 (for all methods and parameter values), along with the average similarity of the
278 nonlinear network estimate by each method with the one obtained for the linear Granger causality
279 method. The linear Granger causality shows the highest reliability, with the average Spearman's rank
280 coefficient ~ 0.6 . The equiquantal binning method provided most reliable network estimates for
281 $Q = 2$ ($\bar{r} \sim 0.36$), with reliability generally decreasing for increasing Q . The k-nearest neighbors
282 algorithm provided even less reliable network estimates, with only weak dependence on the values of
283 the k -parameter and optimum reliability of $\bar{r} \sim 0.33$ for $k = 64$.

284 The causality networks constructed by each nonlinear method have been compared to the causality
285 network obtained using the linear Granger causality analysis, see white bars Figure 1. In general,
286 the nonlinear causality networks have shown higher similarity to linear estimates than to nonlinear
287 estimates for different section of the stationary model time series. Interestingly, the parameter settings
288 that optimized the reliability also provided the (almost) closest results to the linear methods. We have
289 also observed generally lower reliability of the EQQ method for odd Q -values, an effect that will be
290 investigated in detail elsewhere.

291 Figure 2 shows the results of an analogous analysis on original data rather than the stationary model.
292 Note that here the computed causality network similarities reflect a combination of (lack of) reliability
293 of the methods and real variability in the dynamical properties of the time series across time (i.e. true
294 changes in the causality pattern). The results are both qualitatively and quantitatively similar to those

Figure 1. Reliability of causality network detection using different causality estimators, and the similarity to linear causality network estimates: Fourier surrogates model. For each estimator, six causality networks are estimated, one for each decade-long section of model stationary data (a Fourier surrogate realization of the original data). Black: the height of the bar corresponds to the average Spearman's correlation across all 15 pairs of decades. White: the height of the bar corresponds to the average Spearman's correlation of nonlinear causality network and linear causality network across 6 decades.



295 shown in Figure 1, suggesting that the true variability of the causal networks on this time scale is likely
 296 rather small compared to the coarseness of the causality assessment methods.

297 The results for other settings are shown in Figure 3 (use of multivariate AR(1) as the stationary model)
 298 and Figure 4 (6-day averages), generally confirming the main observations. However, some differences
 299 were observable, for instance in the 6-days-averaged data, the reliability dependence of the kNN method
 300 on the k -parameter was more pronounced and peak for a higher value of $k = 256$. The increase of
 301 reliability of the EQQ method for high Q was found to be spurious and is discussed in section 4.

302 3.2. Unweighted causality networks

303 For unweighted causality networks, the after thresholding to keep 1 percent of the strongest links,
 304 the network similarity was assessed by the Jaccard correlation coefficient. The results are plotted
 305 analogously as in the previous figures, see 5.

306 3.3. Components and resulting networks

307 To visualize the climatic networks, we first provide an overview of the localization of the networks in
 308 Figure 6 showing a parcellation of the globe by the components.

309 As an example of causality networks detected, we provide the networks detected by the linear Granger
 310 causality (Figure 7) and the EQQ with $Q = 2$ (Figure 8) for the decade 1948-1957.

311 4. Discussion

Figure 2. Variability of causality network detection using different causality estimators, and the similarity to linear causality network estimates: original data. For each estimator, six causality networks are estimated, one for each decade of the data. Black: the height of the bar corresponds to the average Spearman's correlation across all 15 pairs of decades. White: the height of the bar corresponds to the average Spearman's correlation of nonlinear causality network and linear causality network across 6 decades.

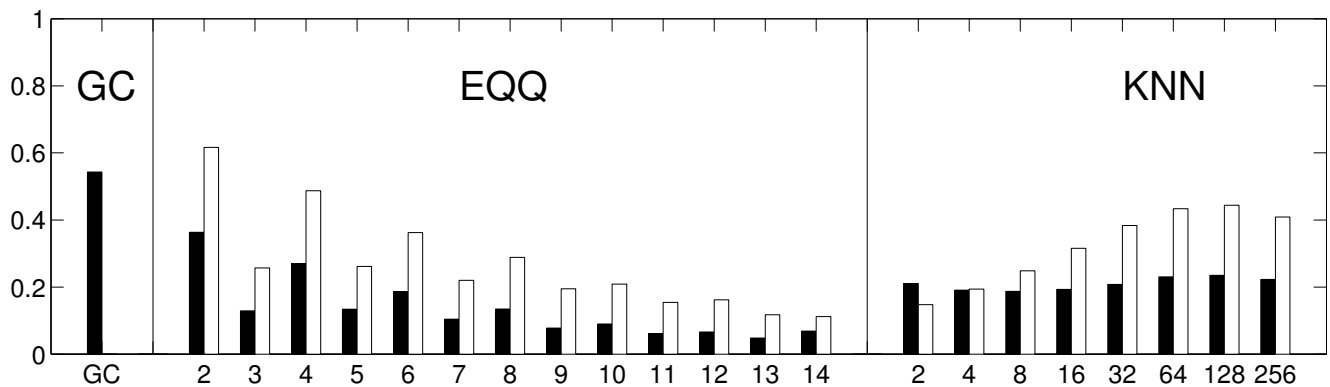


Figure 3. Reliability of causality network detection using different causality estimators, and the similarity to linear causality network estimates, for stationary model constructed as multivariate AR(1) surrogate of the original data. For each estimator, six causality networks are estimated, one for each decade of modeled stationary data. Black: the height of the bar corresponds to the average Spearman's correlation across all 15 pairs of decades. White: the height of the bar corresponds to the average Spearman's correlation of nonlinear causality network and linear causality network across 6 decades.

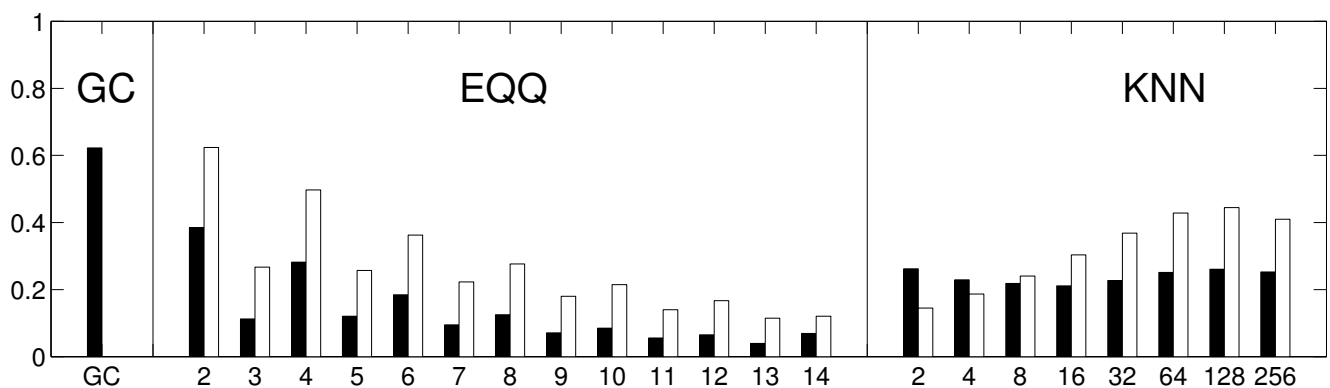


Figure 4. Reliability of causality network detection using different causality estimators, and the similarity to linear causality network estimates, for stationary model constructed as multivariate AR(1) surrogate of the original data. For each estimator, six causality networks are estimated, each for a separate realization of the multivariate AR(1) process fitted to the original data. Black: the height of the bar corresponds to the average Spearman's correlation across all 15 pairs of decades. White: the height of the bar corresponds to the average Spearman's correlation of nonlinear causality network and linear causality network across 6 decades.

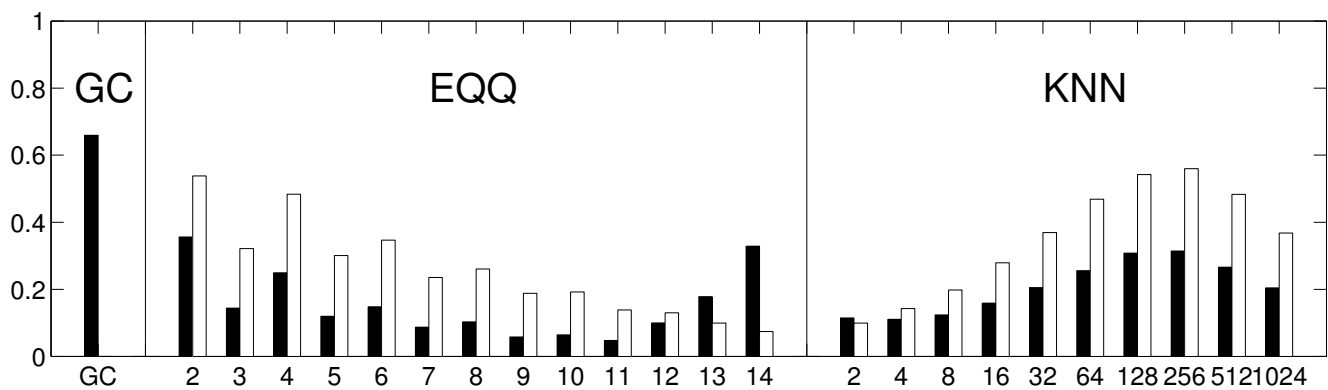


Figure 5. Reliability of causality network detection using different causality estimators, and the similarity to linear causality network estimates. For each estimator, six causality networks are estimated, one for each decade of modeled stationary data. Black: the height of the bar corresponds to the average Jaccard similarity coefficient across all 15 pairs of decades. White: the height of the bar corresponds to the average Jaccard similarity coefficient of nonlinear causality network and linear causality network across 6 decades.

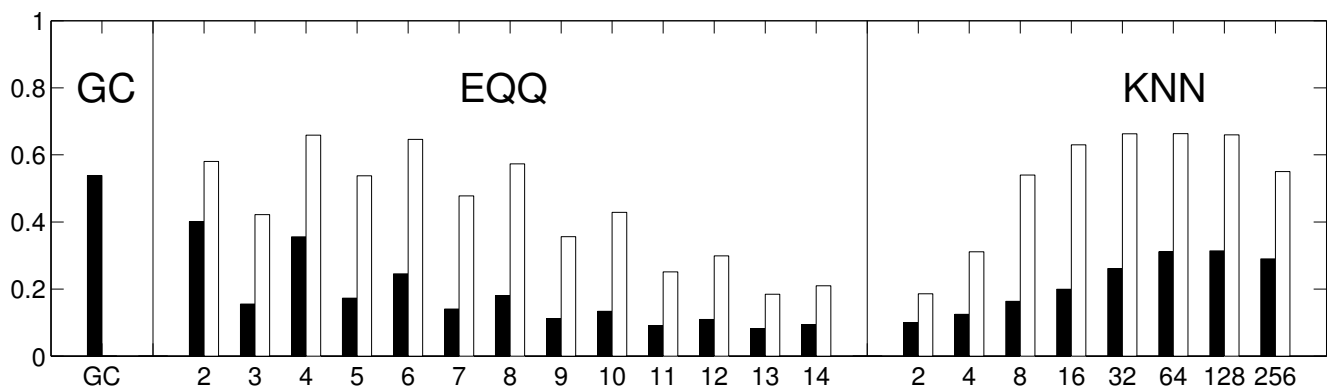


Figure 6. Location of areas dominated by specific components of the climate surface air temperature data VARIMAX-rotated PCA decomposition. For each location, the color corresponding to the component with maximal intensity it used. White dots represent approximate centers of mass of the components, used in subsequent figures for visualization of the nodes of the networks.

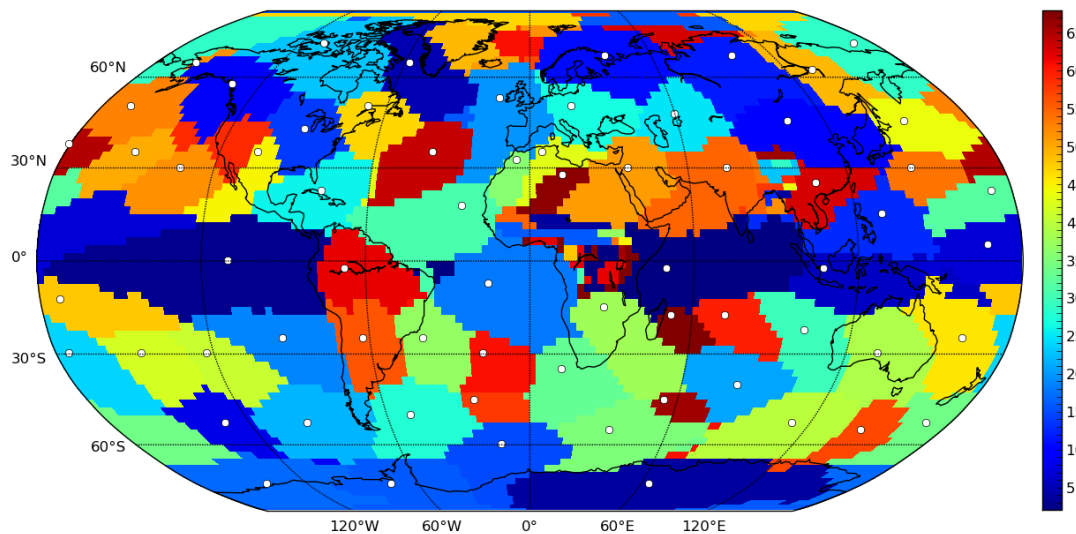


Figure 7. Example of detected causality network, detected by the linear Granger causality for the decade 1948-1957. Links with $\mathcal{T}_{X \rightarrow Y} \geq 0.02$ shown.

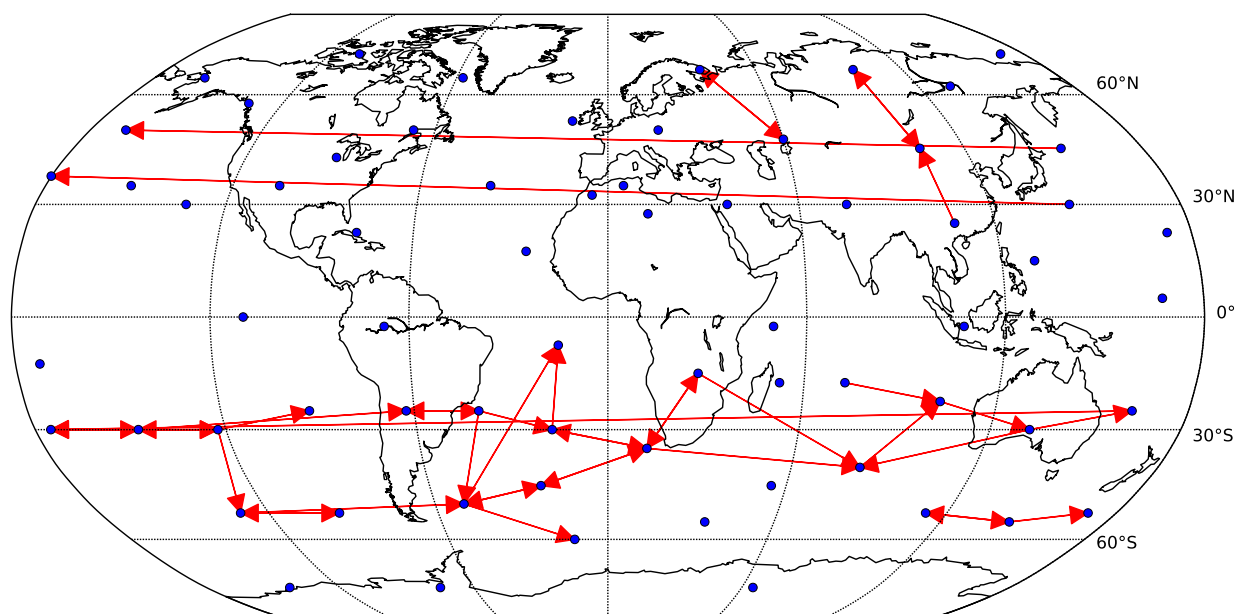
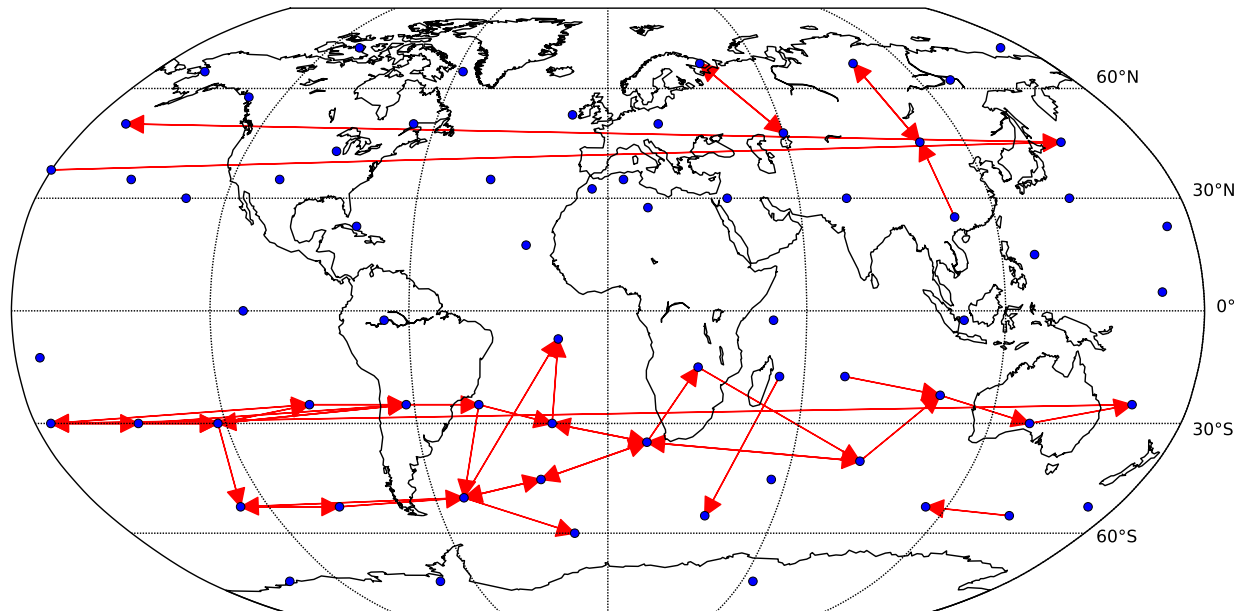


Figure 8. Example of detected causality network, detected by the equiquantal conditional mutual information method with $Q = 2$, for the decade 1948-1957. Density fixed to correspond to density of the network shown in Figure 7.



312 The series of examinations provided evidence that both nonlinear and linear methods may be used
 313 to construct directed climate networks in a reliable way under a range of settings, with the basic linear
 314 Granger causality outperforming the studied nonlinear methods.

315 For the sake of tractability, we have limited the investigation in several ways. On the side of nonlinear
 316 causality methods, we focused on the prominent family of methods based on estimation of conditional
 317 mutual information (transfer entropy). Two algorithms were used that represent key approaches of
 318 estimation of conditional mutual information and have been extensively used and proven efficient on
 319 real-world data. Alternative approaches also exist including the use of recurrence plots [27].

320 The particular pairwise version of linear Granger causality was chosen for its theoretical equivalence
 321 to the transfer entropy (under the assumption of linearity), as this provides a fair comparison.

322 However, the use of the strictly pairwise causality estimators suffers from inherent limitations. To
 323 give an example, a system consisting of three processes X, Y, Z , where Z drives both X and Y , but with
 324 different temporal lags, may erroneously show causal influence between X and Y even if these were
 325 not directly coupled. To deal with such situations, the concepts can be generalized to allow to take into
 326 account the variance explained by third variable(s).

327 Similarly, the assumption of a single possible lag (1 time step of 1 or 6 days respectively in our
 328 investigation) may in real context not be suitable, although at least the relative reliability of different
 329 methods may not be strongly affected by this within reasonable range of parameters.

330 In general, estimation of these generalized causality patterns from relatively short time series is
 331 technically challenging, particularly in the context of nonlinear, information-theory based causality
 332 measures, due to the exponentially increasing dimension of probability distributions to be estimated.

333 However, recent work has provided promising approaches to tackle this curse of dimensionality by
334 decomposing TE into low-dimensional contributions [28]. For theoretical and numerical considerations
335 on how a causal coupling strength can be defined in the multivariate context, see [29].

336 For completeness we mention that apart from the time-domain treatment of causality, the whole
337 problem can also be reformulated in the spectral domain, leading to frequency-resolved causality indices
338 such as partial directed coherence (PDC, [30]) or Directed Transfer Function (DTC, [31]).

339 The study also shows some key properties of the conditional mutual information estimates. Note that
340 for instance for the 6-days networks (Figure 4), the EQQ method reliability increases again for $Q \geq 11$,
341 however, the similarity to the linear estimate further decreases. A direct check of the causality networks
342 shows that they tend to a trivial column-wise structure, with the intensities for each column highly
343 correlated to the autoregressive coefficient of the given time series. This corresponds to a manifestation
344 of a dominant autocorrelation-dependent bias in the EQQ estimator for too high Q values (note that
345 $Q = 14$ corresponds to less than one time point per average in a 4D bin, an unsuitable sampling of the
346 space for effective probability distribution function approximation).

347 Reconstruction of networks directly from gridded climatic field data is a challenging and perhaps not
348 always the best approach, for reasons including efficient computation and visualization of the results.
349 Instead, we apply here a decomposition of the data in order to get the most important components, i.e.,
350 by using a varimax-rotated principle component analysis. This provides a useful dimension-reduction of
351 the studied problem. In particular, the gridded data does not reflect the real climate subsystems, which
352 may be better approximated by the decomposition modes. However, as the decomposition is an implicit
353 (weighted) coarse-graining, the detected difference between the linear and nonlinear methods may be
354 different from that in the original time series data. In particular, the spatial averaging may increase
355 the reliability of both approaches by suppressing noise, but also suppress any highly spatially localized
356 heterogeneous patterns of both nonlinear and linear character. This might be reflected in the specific
357 results of the paper, in particular the obtained quantitative reliability estimates.

358 In general, the differences in reliability may have important consequences for the detectability of
359 causal links as well as of their changes. Of course, theoretically this is not necessary as in a particularly
360 nonlinear system links may exist that would have negligible linear causality component, but their
361 nonlinear causality fingerprint would be strong enough to be detected. Recent works have proposed
362 approaches for explicit quantification of the nonlinear contribution of equal-time dependence [32] and
363 applied them to neuroscientific [32] as well as climate data [10]. However, the generalization of the
364 approach to higher dimension information-theoretic functionals is not straightforward and is subject of
365 ongoing work. Thus, we give here at least an illustrative example of the practical result of trade-off
366 between generality of transfer entropy and higher reliability of linear Granger causality: using the
367 original 67 components data (divided into 6 decadal sections, see section 2), the basic statistical test
368 at the 5 percent significant level (described in the 2 section) marked on average 1592 links as statistically
369 significant (out of 4422 possible), while the EQQ method showed in general a lower number of significant
370 links, dependent on the parameter value in a way similar to the reliability estimate, with maximum of
371 983 significant links for $Q = 2$ and minimum of 287 significant links for $Q = 13$. Note that given the
372 significance level of the test, on average $221 \approx 4422 * 0.05$ significant links would be expected to appear
373 by chance in a collection of completely unrelated processes.

374 5. Conclusions

375 Meaningful interpretation of climate networks and their observed temporal variability requires
376 knowledge and minimization of the methodological limitations of the methods of their construction.
377 In the presented work, we discussed the problem of reliability of network construction from time series
378 of finite length, quantitatively assessing the reliability for a selection of standard bivariate causality
379 methods. These included two major algorithms for estimating transfer entropy with a wide range of
380 parameter choices, as well as the linear Granger causality analysis, which can be understood as linear
381 approximation of transfer entropy. Overall, causality methods provided reproducible estimates of climate
382 causality networks, with the linear approximations outperforming in reliability the studied nonlinear
383 methods. Interestingly, optimizing the nonlinear methods with respect to reliability has led to improved
384 similarity of the detected networks to those discovered by linear methods, in line with the hypothesis of
385 near-linearity of the investigated climate reanalysis data, in particular the surface air temperature time
386 series.

387 The latter hypothesis regarding the surface air temperature has been supported by the study in [10]
388 which extended the older results of [33] who tested for possible nonlinearity in the dynamics of the
389 station (Prague-Klementinum) SAT time series and found that the dependence between the SAT time
390 series $x(t)$ and its lagged twin $x(t + \tau)$ was well-explained by a linear stochastic process. This result
391 about a linear character of the temporal evolution of SAT time series, as well as the results of this
392 study about causal relations between the principal components obtained from the reanalysis SAT time
393 series cannot be understood as arguments for a linear character of atmospheric dynamics *per se*. Rather,
394 these results characterize properties of measurement or reanalysis data at a particularly coarse level of
395 resolution, when the data reflecting a spatially and temporally averaged mixture of dynamical processes
396 on a wide range of spatial and temporal scales are considered. For instance, a closer look on the dynamics
397 on specific temporal scales in temperature and other meteorological data has led to identification of
398 oscillatory phenomena with nonlinear behavior, exhibiting phase synchronization [34–38]. Also the
399 leading modes of atmospheric variability exhibit nonlinear behavior [39,40] and can influence important
400 seasonal circulation phenomena in a nonlinear way [41].

401 Further work is needed to assess the usability and advantages of more sophisticated, recently proposed
402 causality estimation methods. The current work also provides an important step towards reliable
403 characterization of climate networks and detection of potential changes over time.

404 Acknowledgements

405 This study is supported by the Czech Science Foundation, Project No. P103/11/J068 and by the DFG
406 grant No. KU34-1.

407 References

- 408 1. Newman, M.E.J. The structure and function of complex networks. *SIAM Review* **2003**, *45*, 167–
409 256.
- 410 2. Boccaletti, S.; Latora, V.; Moreno, Y.; Chavez, M.; Hwang, D.U. Complex networks: Structure
411 and dynamics. *Physics Reports* **2006**, *424*, 175–308.

- 412 3. Tsonis, A.; Roebber, P. The architecture of the climate network. *Physica A* **2004**, *333*, 497–504.
- 413 4. Tsonis, A.A.; Swanson, K.L.; Roebber, P.J. What do networks have to do with climate? *Bulletin*
414 *of the American Meteorological Society* **2006**, *87*, 585+.
- 415 5. Yamasaki, K.; Gozolchiani, A.; Havlin, S. Climate networks around the globe are significantly
416 affected by El Nino. *Physical Review Letters* **2008**, *100*.
- 417 6. Malik, N.; Bookhagen, B.; Marwan, N.; Kurths, J. Analysis of spatial and temporal extreme
418 monsoonal rainfall over South Asia using complex networks. *Climate Dynamics* **2012**, *39*, 971–
419 987.
- 420 7. Steinhäuser, K.; Ganguly, A.R.; Chawla, N.V. Multivariate and multiscale dependence in the
421 global climate system revealed through complex networks. *Climate Dynamics* **2012**, *39*, 889–
422 895.
- 423 8. Donges, J.F.; Zou, Y.; Marwan, N.; Kurths, J. The backbone of the climate network. *EPL* **2009**,
424 *87*, 48007.
- 425 9. Donges, J.F.; Zou, Y.; Marwan, N.; Kurths, J. Complex networks in climate dynamics. *European*
426 *Physical Journal* **2009**, *174*, 157–179.
- 427 10. Hlinka, J.; Hartman, D.; Vejmelka, M.; Novotna, D.; Paluš, M. Non-linear dependence and
428 teleconnections in climate data: sources, relevance, nonstationarity. *submitted*.
- 429 11. Granger, C.W. Investigating causal relations by econometric model and cross-spectral methods.
430 *Econometrica* **1969**, *37*, 414–&.
- 431 12. Vejmelka, M.; Palus, M. Inferring the directionality of coupling with conditional mutual
432 information. *Physical Review E (Statistical, Nonlinear, and Soft Matter Physics)* **2008**, *77*.
- 433 13. Schreiber, T. Measuring information transfer. *Physical Review Letters* **2000**, *85*, 461–464.
- 434 14. Kistler, R.; Kalnay, E.; Collins, W.; Saha, S.; White, G.; Woollen, J.; Chelliah, M.; Ebisuzaki,
435 W.; Kanamitsu, M.; Kousky, V.; van den Dool, H.; Jenne, R.; Fiorino, M. The NCEP-NCAR
436 50-year reanalysis: Monthly means CD-ROM and documentation. *Bulletin of the American*
437 *Meteorological Society* **2001**, *82*, 247–267.
- 438 15. Kalnay, E.; Kanamitsu, M.; Kistler, R.; Collins, W.; Deaven, D.; Gandin, L.; Iredell, M.; Saha, S.;
439 White, G.; Woollen, J.; Zhu, Y.; Chelliah, M.; Ebisuzaki, W.; Higgins, W.; Janowiak, J.; Mo, K.;
440 Ropelewski, C.; Wang, J.; Leetmaa, A.; Reynolds, R.; Jenne, R.; Joseph, D. The NCEP/NCAR
441 40-year reanalysis project. *Bulletin of the American Meteorological Society* **1996**, *77*, 437–471.
- 442 16. Wiener, N., *Modern Mathematics for Engineers*; McGraw-Hill, New York, 1956; chapter The
443 theory of prediction, pp. 165 – 190.
- 444 17. Ding, M.; Chen, Y.; Bressler, S.L., *Granger Causality: Basic Theory and Application to*
445 *Neuroscience*. In *Handbook of Time Series Analysis*; Wiley-VCH Verlag GmbH & Co. KGaA,
446 2006; pp. 437–460.
- 447 18. Geweke, J.F. Measurement of linear dependence and feedback between multiple time series.
448 *Journal of the American Statistical Association* **1982**, *77*, 77.
- 449 19. Geweke, J.F. Measures of Conditional Linear Dependence and Feedback Between Time Series.
450 *Journal of the American Statistical Association* **1984**, *79*, 907–915.
- 451 20. Barnett, L.; Barrett, A.B.; Seth, A.K. Granger Causality and Transfer Entropy Are Equivalent for
452 Gaussian Variables. *Physical Review Letters* **2009**, *103*.

- 453 21. Palus, M.; Albrecht, V.; Dvorak, I. Information theoretic test for nonlinearity in time series.
454 *Physics Letters A* **1993**, *175*, 203–209.
- 455 22. Kaiser, H. The varimax criterion for analytic rotation in factor analysis. *Psychometrika* **1958**,
456 *23*, 187–200.
- 457 23. Schwarz, G. Estimating the dimension of a model. *The Annals of Statistics* **1978**, *5*, 461–464.
- 458 24. Benjamini, Y.; Hochberg, Y. Controlling the false discovery rate: a practical and powerful
459 approach to multiple testing. *Journal Of The Royal Statistical Society Series B-methodological*
460 **1995**, *57*, 289–300.
- 461 25. Prichard, D.; Theiler, J. Generating surrogate data for time series with several simultaneously
462 measured variables. *Physical Review Letters* **1994**, *73*, 951.
- 463 26. Palus, M. Detecting phase synchronization in noisy systems. *Physics Letters A* **1997**, *235*, 341–
464 351.
- 465 27. Zou, Y.; Romano, M.C.; Thiel, M.; Marwan, N.; Kurths, J. Inferring indirect coupling by means
466 of recurrences. *International Journal Of Bifurcation And Chaos* **2011**, *21*, 1099–1111.
- 467 28. Runge, J.; Heitzig, J.; Petoukhov, V.; Kurths, J. Escaping the Curse of Dimensionality in
468 Estimating Multivariate Transfer Entropy. *Physical Review Letters* **2012**, *108*.
- 469 29. Runge, J.; Heitzig, J.; Marwan, N.; Kurths, J. Quantifying causal coupling strength: A lag-
470 specific measure for multivariate time series related to transfer entropy. *Physical Review E* **2012**,
471 *86*.
- 472 30. Baccala, L.A.; Sameshima, K. Partial directed coherence: a new concept in neural structure
473 determination. *Biological Cybernetics* **2001**, *84*, 463–474.
- 474 31. Kaminski, M.; Ding, M.; Truccolo, W.A.; Bressler, S.L. Evaluating causal relations in neural
475 systems: Granger causality, directed transfer function and statistical assessment of significance.
476 *Biol Cybern* **2001**, *85*, 145–157.
- 477 32. Hlinka, J.; Palus, M.; Vejmelka, M.; Mantini, D.; Corbetta, M. Functional connectivity in resting-
478 state fMRI: Is linear correlation sufficient? *NeuroImage* **2011**, *54*, 2218–2225.
- 479 33. Palus, M.; Novotna, D. Testing for nonlinearity in weather records. *Physics Letters A* **1994**,
480 *193*, 67–74.
- 481 34. Palus, M.; Novotna, D. Enhanced Monte Carlo Singular System Analysis and detection of period
482 7.8 years oscillatory modes in the monthly NAO index and temperature records. *Nonlinear*
483 *Processes in Geophysics* **2004**, *11*, 721–729.
- 484 35. Palus, M.; Novotna, D. Quasi-biennial oscillations extracted from the monthly NAO index and
485 temperature records are phase-synchronized. *Nonlinear Processes in Geophysics* **2006**, *13*, 287–
486 296.
- 487 36. Palus, M.; Novotna, D. Phase-coherent oscillatory modes in solar and geomagnetic activity and
488 climate variability. *Journal of Atmospheric and Solar-terrestrial Physics* **2009**, *71*, 923–930.
- 489 37. Palus, M.; Hartman, D.; Hlinka, J.; Vejmelka, M. Discerning connectivity from dynamics in
490 climate networks. *Nonlinear Processes in Geophysics* **2011**, *18*, 751–763.
- 491 38. Feliks, Y.; Ghil, M.; Robertson, A.W. Oscillatory Climate Modes in the Eastern Mediterranean
492 and Their Synchronization with the North Atlantic Oscillation. *Journal of Climate* **2010**,
493 *23*, 4060–4079.

- 494 39. Boucharel, J.; Dewitte, B.; du Penhoat, Y.; Garel, B.; Yeh, S.W.; Kug, J.S. ENSO nonlinearity in
495 a warming climate. *Climate Dynamics* **2011**, *37*, 2045–2065.
- 496 40. Osprey, S.M.; Ambaum, M.H.P. Evidence for the chaotic origin of Northern Annular Mode
497 variability. *Geophysical Research Letters* **2011**, *38*.
- 498 41. Mokhov, I.I.; Smirnov, D.A.; Nakonechny, P.I.; Kozlenko, S.S.; Seleznev, E.P.; Kurths, J.
499 Alternating mutual influence of El-Nino/Southern Oscillation and Indian monsoon. *Geophysical*
500 *Research Letters* **2011**, *38*.

501 © January 29, 2013 by the authors; submitted to *Entropy* for possible open access
502 publication under the terms and conditions of the Creative Commons Attribution license
503 <http://creativecommons.org/licenses/by/3.0/>.